Spectroscopy and efficient laser operation near 1.95 μm of Tm^{3+} in disordered $NaLu(WO_4)_2$

Xiumei Han,[1] José M. Cano-Torres,[1] Mauricio Rico,[1] Concepción Cascales,[1] Carlos Zaldo,[1,a)] Xavier Mateos,[2,b)] Simon Rivier,[2] Uwe Griebner,[2] and Valentin Petrov[2]
[1]*Instituto de Ciencia de Materiales de Madrid, Consejo Superior de Investigaciones Científicas, c/ Sor Juana Inés de la Cruz 3, 28049 Madrid, Spain*
[2]*Max-Born-Institute for Nonlinear Optics and Ultrafast Spectroscopy, 2A Max-Born-Strasse, D-12489 Berlin, Germany*

(Received 3 December 2007; accepted 14 February 2008; published online 22 April 2008)

Continuous wave and tunable laser operation at room temperature is demonstrated with single crystals of Tm-doped $NaLu(WO_4)_2$. Under Ti:sapphire laser pumping and tuning by an intracavity Lyot filter, the Tm^{3+} emission extended from 1799 to 2026 nm. The maximum output power exceeded 0.5 W and the maximum slope efficiency with respect to the absorbed power was above 58%. These good laser properties are related to the locally disordered tetragonal ($I\bar{4}$) structure of the crystalline host. Using low temperature spectroscopy and energy level simulation methods, the energy levels and spectroscopic properties of Tm^{3+} have been shown to be compatible with the S_4 site symmetry. This allowed the reliable determination of the emission cross sections related to the laser transitions. © *2008 American Institute of Physics*. [DOI: 10.1063/1.2907438]

I. INTRODUCTION

Tm^{3+} is a lanthanide ion of interest for diode-pumped laser emission which can extend, depending on the host, from below 1.9 to above 2 μm. Tm lasers have been demonstrated with a number of fluoride and oxide crystals with ordered or disordered structure,[1] see Tables I and III therein. The $^3H_6 \rightarrow {}^3H_4$ transition of Tm^{3+} efficiently absorbs the ~800 nm emission of AlGaAs diode lasers, however, due to the limited number of wavelengths from commercially available high power diode lasers, the pumping is often nonoptimized. In this respect, hosts which provide broader bandwidths of the Tm^{3+} spectral lines relax the requirements to the pump source and reduce the sensitivity to thermal drifts of the pump wavelength. Broader emission lines are, on the other hand, advantageous for tunable and mode-locked laser operation. The main disadvantage of Tm^{3+} as a quasi-three-level system for the $^3F_4 \rightarrow {}^3H_6$ laser transition is the thermal population of the terminal level which belongs to the ground state multiplet. As a consequence, the laser performance critically depends on the operation temperature and host properties such as crystal field strength and ion-host interactions. Moreover, Tm–Tm interactions can also give rise to nonradiative losses.

Some of the tetragonal double tungstates (DTs) with nominal formula $M^+T^{3+}(WO_4)_2$ (shortly MTW) and with the structure of the $I\bar{4}$ space group have been recently shown to be efficient hosts for Yb lasers, e.g., Refs. 2–4. The local structural disorder associated with the monovalent and trivalent cation occupancies of the same lattice sites results in inhomogeneous spectral line broadening for the optical transitions. This property is the base for the good tunability of the Yb^{3+} laser emission and for the ultrashort pulse durations obtained, down to 53 fs in Yb:NaYW.[4] Some previous studies dealt with spectroscopic properties of Tm^{3+} in tetragonal NaGdW,[5–8] NaLaW,[9,10] NaBiW,[11] and in the isostructural double molybdates (DMos) NaLaMo[12] and KLaMo.[13] These studies evidenced the difficulties in establishing the correct energy level sequence for Tm^{3+} solely from the experimental spectroscopic data because of the broad bands observed, even at cryogenic temperatures, and the uncertainty in the determination of the number of bands and their polarization nature. All these problems lead to errors in the evaluation of the spectroscopic parameters involved in laser operation, e.g., the $^3F_4$ and $^3H_6$ partition functions. So far, Tm^{3+} laser operation has been demonstrated only in NaGdW[5,7] and in NaLaW.[9]

Four trivalent rare-earth ions are commonly used to grow transparent rare-earth based laser hosts of the DT and DMo types, namely, Y, La, Gd, and Lu. From these, Y and Lu with the smallest ionic radii lead to stronger crystal fields exerted on the optically active Tm^{3+} dopant, and therefore, they are expected to produce the largest splitting of the ground $^3H_6$ multiplet. The purpose of the present work is to evaluate the spectroscopic and laser properties of Tm^{3+} in single crystals of NaLuW and to compare these properties to previous reports on isostructural DT and DMo Tm hosts.

II. CRYSTAL GROWTH

NaLuW melts with decomposition. We have grown Tm-doped single crystals of this compound by using the top seeded solution growth (TSSG) slow cooling method without pulling. The starting products were WO_3 (99+% from Aldrich), Na_2CO_3 (99.5% from Alfa Aesar), Tm_2O_3 (99.99%), and Lu_2O_3 (99.99%), the last two of which were purchased through Shanghai Zimei International Trade Co. Ltd. The

a)Electronic mail: cezaldo@icmm.csic.es.
b)Present address: Física i Cristal.lografia de Materials (FiCMA), Universitat Rovira i Virgili. Campus Sescelades c/Marcel.lí Domingo, s/n, E-43007 Tarragona, Spain.

TABLE I. Conditions used to grow Tm:NaLuW crystals by the TSSG method. T_{seed} is the crystal nucleation temperature and ΔT is the growth cooling interval. [Tm] is the dopant concentration in the melt or in the crystal.

$[Tm]_{melt}$ (mol %)	Solvent	Solute/solvent (mol/mol)	T_{seed} (°C)	ΔT (°C)	$[Tm]_{crystal}$ (mol %)	$[Tm]_{crystal}$ (10^{20} cm^{-3})
10	$Na_2W_2O_7$	1/7.2	913.5	5.5	11.72	7.85
5	1 Na_2WO_4:1 $Na_2W_2O_7$	1/9	885	17	5.86	3.92

flux was either $Na_2W_2O_7$ for 10 mol % Tm doping or a 1:1 mol mixture of Na_2WO_4 and $Na_2W_2O_7$ for 5 mol % Tm doping. Mixtures of Tm-doped NaLuW (solute) and the flux (solvent), in the ratios given in Table I, were melted in 70 cm^3 platinum crucibles. The cooling rate during the growth was 0.05 °C/h. The seed rotation rate was at 35 rpm. Table I summarizes some details of the growth process. After growth, the crystals were slowly cooled to 25 °C following several ramps with increasing temperature slopes: 5 °C/h in the 868–746 °C range, 10 °C/h in the 746–601 °C range, and 15 °C/h down to 25 °C.

Crystals of NaGdW with *c* cut were used as seed. The Tm:NaLuW crystals nucleated and grew on the seed forming a pyramid of square base [see Fig. 1(a)]. The side dimension of the pyramid base was typically in the 10–15 mm range. The crystals were oriented by Laue x-ray diffraction techniques and *a*-cut plates with different thicknesses were sliced and polished for polarized optical spectroscopy and laser experiments. Figure 1(b) shows a typical sample used for spectroscopic and laser experiments.

The Tm concentration in the crystal, $[Tm]_{crystal}$, was determined by x-ray fluorescence spectroscopy using a Philips equipment, model MagiX Super Q, with a 2.4 kW Rh x-ray generator. Ground 10 mol % Tm-doped single crystal and Tm_2O_3–Lu_2O_3–Na_2CO_3–WO_3 powder mixtures with different Tm and Lu contents were melted in $Li_2B_4O_7$ to eliminate particle size effects. The latter were used to build independent calibration curves for Na, Lu, Tm, and W. The $K\alpha$ (for Na) and $L\alpha_1$ (for Lu, Tm, and W) x-ray emissions were diffracted by a LiF 200 crystal analyzer using a 150 μm collimator. The crystal formula obtained is $Na_{0.973}Lu_{0.947}Tm_{0.117}(W_{1.022}O_4)_2$. The Tm concentration in the other crystal was calculated by comparing the intensity of the Tm^{3+} optical absorption. The Tm segregation coefficient defined as the ratio between the molar concentration in the crystal and in the melt is $S \approx 1.1$. The Tm density in the crystal, also included in Table I, was calculated using the NaLuW cell volume [$V=298.82$ Å^3 (Ref. 14)].

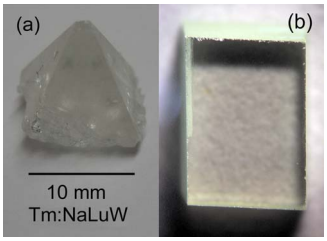

FIG. 1. (Color online) (a) Tm:NaLuW crystal as grown by the TSSG slow cooling method. (b) Polished *a*-cut sample (aperture of 4×3 mm^2) used in the spectroscopic and laser experiments.

III. SPECTROSCOPIC STUDIES

Polarized (σ, $\boldsymbol{B}\|c$ axis and π, $\boldsymbol{E}\|c$ axis) optical spectroscopy of Tm^{3+} has been performed from 5 to 300 K using a closed-cycle He cryostat. Optical absorption (OA) spectra were recorded in a Varian spectrophotometer, model Cary 5E. The photoluminescence (PL) was excited with a cw Ti:sapphire laser modulated by a chopper (≈200 Hz), dispersed by a SPEX spectrometer ($f=34$ cm), and detected with a 77 K cooled InSb photovoltaic detector (Hamamatsu, model P5968-060) connected to a lock-in amplifier.

Figure 2 shows the ground state OA and PL measurements at 5 K. The spectra are characterized by pronounced polarization dependence and broad bandwidths. Although some of the possible environments associated with the random distribution of the Na and Lu in 2*b* and 2*d* crystal sites reduce the S_4 local symmetry to C_2 or even C_1,[15] we ana-

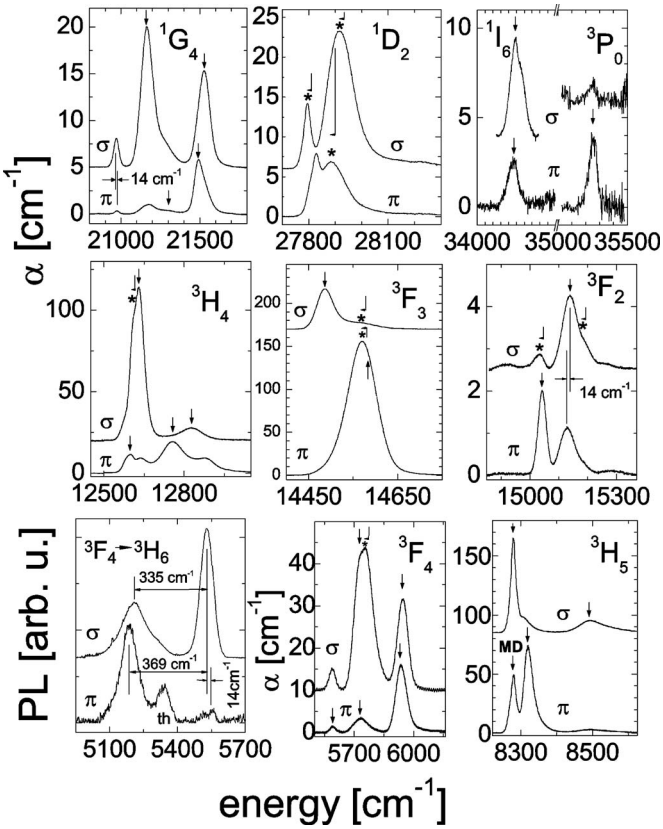

FIG. 2. 5 K polarized (σ or π) optical absorption (α) and photoluminescence (PL) of 11.72 mol % Tm-doped NaLuW single crystal. The photoluminescence was excited at 793.3 nm. Bands due to transitions from the $^3H_6(1)$ level are labeled with *, the energy corresponding to the excited level (most often Γ_2) is labeled with ←. Other selected bands are labeled with ↓. MD indicates magnetic dipole contribution. Th indicates the thermal assisted bands.

lyzed the Tm^{3+} spectroscopy by assuming an average Tm center in S_4 symmetry which should correspond to the majority of Tm centers in NaLuW. In this symmetry, the Stark energy levels are labeled with three irreducible representations (IRs), Γ_1, Γ_2, and $\Gamma_{3,4}$, the last one being double degenerated. The electric dipole (ED) and magnetic dipole (MD) transition rules can be found in a previous work.[5] The most difficult issue in the interpretation of the present data is in determining the IR of the Stark level with the lowest energy, i.e., $^3H_6(0)$. Generally, lack of an accessible excited singlet ($J=0$) or the uncertainty in its assignment prevents the deduction of the $^3H_6(0)$ IR from experimental data. The identification of possible bands related to excited $^3H_6(0)$ Stark levels close in energy to the lowest one presents another difficulty in the interpretation of the spectra. The spectroscopic analysis is further complicated by the fact that ED $\Gamma_1 \rightarrow \Gamma_1$ and $\Gamma_2 \rightarrow \Gamma_2$ transitions are forbidden, therefore, the number of optical bands observed at low temperature is expected to be smaller than the number of excited levels.

The construction of the energy level scheme from the low temperature spectroscopic measurements is largely facilitated by an initial crystal field (CF) simulation of these energy levels using parameters for Tm^{3+}, which were previously determined in other isostructural hosts, such as the tetragonal scheelite $CaWO_4$ crystal,[16] or extrapolating CF parameters of other rare-earth dopants in isostructural crystals, e.g., those of Er^{3+} in NaBiW.[17] Such a theoretical calculation for Tm in NaLuW was performed by procedures previously described[18] by using the free ion (FI) parameters for Tm^{3+} determined earlier.[19] It yielded an $^3H_6$ lowest level having a Γ_2 IR, which is in agreement with previous results reported for other S_4 Tm^{3+} centers in isostructural hosts,[16,20,21] and consistent with the present polarized measurements. In particular, the presence in the π OA spectrum of a well resolved band at 35 254 cm^{-1} is consistent with its assignment to the $^3P_0$ level, since $J=0$ implies a Γ_1 IR, and therefore, it fulfills the selection rule for $\Gamma_2 \rightarrow \Gamma_1$ transition in the S_4 symmetry. Thus, the present combination of experimental and simulated results allows the full rationalization and assignment of the observed transitions.

Experimental evidence of the relative energies of some $^3H_6(n)$ Stark levels was obtained from the study of the thermal evolution of the polarized spectra corresponding to the $^3H_6 \rightarrow {}^3H_5$ and $^3H_6 \rightarrow {}^3F_3$ OA transitions shown in Figs. 3 and 4, as well as from the PL results included in Fig. 2. Since $\Delta J=1$ holds for $^3H_6 \rightarrow {}^3H_5$ transitions, MD contributions are also expected. This is the reason why some of these bands are seen in σ and π spectra. With increasing sample temperature, the intensity of the band at 8278 cm^{-1} decreases and a new band emerges at an energy of 14 cm^{-1} below the previous one (Fig. 3). We assign this energy difference to the relative energy of the first excited $^3H_6(1)$ level. Similar studies of the $^3F_3$ OA, Fig. 4, provide evidence of $^3H_6(n)$ levels at 65, 266, and 369 cm^{-1}. The latter results are further confirmed by the $^3F_4 \rightarrow {}^3H_6$ PL spectra indicating $^3H_6(n)$ levels at 335 and 369 cm^{-1} (Fig. 2). The remaining energy levels observed, up to a total of 39, were established by applying the ED transition rules to the 5 K OA spectra and consistent comparison with the simulated scheme. Afterward, a fit minimizing the energy differences between observed and calculated levels was carried out through the simultaneous treatment of both FI and CF interactions in a single-electron Hamiltonian for the entire set of $4f^{12}$ Tm^{3+} wave functions.

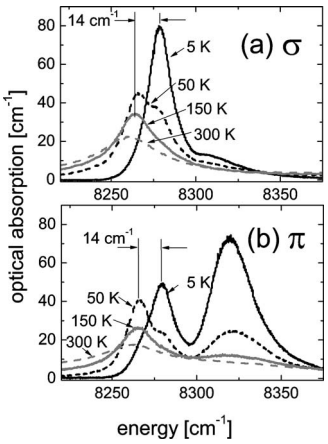

FIG. 3. Polarized optical absorption spectra of the $^3H_5$ multiplet of Tm^{3+} in NaLuW ($[Tm]_{crystal}=11.72$ mol %) for several sample temperatures.

The correspondence between bands and level energies is indicated in Fig. 2. Although the fit provided all energy levels for Tm^{3+} in NaLuW, for the sake of brevity, Table II summarizes only the observed and calculated energies and the IRs of the multiplets of interest for the $^3F_4 \rightarrow {}^3H_6$ laser emission. Table III shows the FI and CF parameters of the best fit and their comparison to those obtained for Tm^{3+} in other crystals, namely, $CaWO_4$,[16] $LiTmF_4$,[20] and $LiYF_4$.[21]

Figure 5(a) shows the $^3H_4$ absorption cross sections $\sigma_{abs}=\alpha/[Tm]$; this is the transition from the ground state that is used for diode pumping. The absorption cross sections for both polarizations have a peak at 795.5 nm, but for σ polarization, the absorption is roughly 2.5 times higher: the maximum values amount to $\sigma_{abs}=3.98\times10^{-20}$ cm^2 (σ polarization) and 1.60×10^{-20} cm^2 (π polarization). The absorption

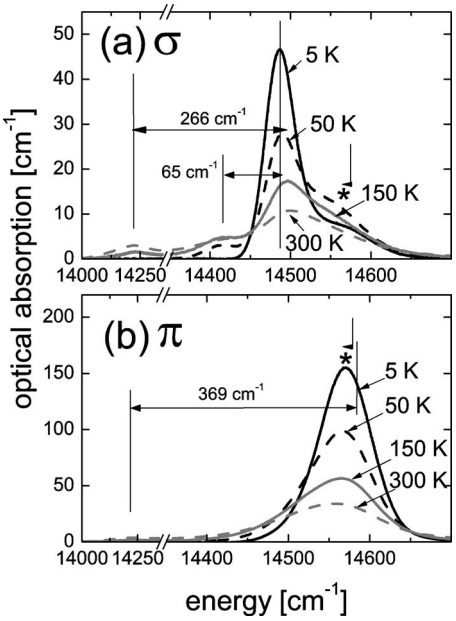

FIG. 4. Polarized optical absorption spectra of the $^3F_3$ multiplet of Tm^{3+} in NaLuW ($[Tm]_{crystal}=11.72$ mol %) for several sample temperatures.

TABLE II. Observed (E_o) and calculated (E_c) energy levels, in cm^{-1}, of Tm^{3+} in NaLuW. IR indicates the corresponding irreducible representation.

$^3H_6(n)$	n	0	1	2	3	4	5	6	7	8	9
	IR	Γ_2	$\Gamma_{3,4}$	Γ_1	Γ_2	Γ_2	Γ_1	$\Gamma_{3,4}$	$\Gamma_{3,4}$	Γ_1	Γ_2
	E_o	0	14	65	⋯	266	⋯	335	⋯	⋯	369
	E_c	−1	23	47	241	275	328	332	378	383	392
$^3F_4(n')$	n'	0′	1′	2′	3′	4′	5′	6′			
	IR	Γ_1	$\Gamma_{3,4}$	Γ_1	Γ_2	Γ_1	Γ_2	$\Gamma_{3,4}$			
	E_o	5591	5724	5730	5774	5931	⋯	5947			
	E_c	5582	5724	5737	5775	5917	5931	5939			

cross sections of the $^3F_4$ multiplet are shown in Fig. 5(b). The emission cross sections of the $^3F_4 \rightarrow {}^3H_6$ laser channel can be obtained from the $^3F_4$ absorption cross sections by using the reciprocity method:

$$\sigma_{\text{emi}} = \sigma_{\text{abs}} \frac{Z_l}{Z_u} e^{(E_{\text{zl}} - h\nu)/k_B T}.$$

$E_{\text{zl}}=5591\ cm^{-1}$ is the zero line energy determined in Table II and $Z_{l,u}=\Sigma_k g_k \exp(-E_k/k_BT)$ are the partition functions of the $^3H_6$ and $^3F_4$ multiplets, where g_k is the level degeneracy, E_k is the energy difference with respect to the lowest Stark level, k_B is the Boltzmann constant, and T is the temperature. By using the energies E_k from Table II, the corresponding partition functions are $Z_l(^3H_6)=5.39$ and $Z_u(^3F_4)=3.74$, i.e., $Z_l/Z_u=1.44$. Figure 5(b) shows the comparison of the calculated emission cross sections with the experimental PL. The agreement between the relative shape of the calculated cross sections and the experimental PL indicates that reabsorption effects were not significant in the PL measurements. The peak values for σ and π polarizations are $\sigma_{\text{emi}} = 2.0(\pm 0.1) \times 10^{-20}\ cm^2$ (at 1798 nm) and $1.9(\pm 0.1) \times 10^{-20}\ cm^2$ (at 1830 nm), respectively.

In view of the good correspondence with the experimental PL, we used the emission cross sections to calculate the radiative lifetime of the $^3F_4$ multiplet by the Füchtbauer–Ladenburg equation, $1/\tau_{\text{rad}} = 8\pi n^2 \int [\langle \sigma_{\text{emi}}(\nu) \rangle / \lambda^2] d\nu$, where the averaging is over the polarization.[22] The NaLuW refractive index n is only known for the 300–1000 nm range.[3] We estimated its value in the 1.8–2.0 μm region as $n=1.92$ by extrapolation. With this assumption, we obtained $\tau_{\text{rad}} = 1.27$ ms. The fluorescence lifetime was measured by the pinhole method[23] by using a 207 μm thick plate of a 5.86 mol % Tm-doped NaLuW crystal. The lifetime obtained under these conditions was 1.20 ms. This experimental value is consistent with the calculated radiative lifetime τ_{rad}.

As was already mentioned, the Tm^{3+} laser operates on the $^3F_4 \rightarrow {}^3H_6$ transition as a quasi-three-level system, and therefore, its efficiency critically depends on the population of the ground state. A first rough estimation of the laser capability is provided by the gain cross sections, $\sigma_{\text{gain}}(\lambda) = \beta\sigma_{\text{emi}}(\lambda) - (1-\beta)\sigma_{\text{abs}}(\lambda)$, where β represents the ratio of the Tm ions in the excited state to the total ion density. σ_{gain} is plotted in Fig. 6 for both polarizations. The expected oscillation wavelength in the absence of frequency selective elements in the laser cavity depends on the inversion ratio (or the cavity losses basically associated with the output coupler). The gain cross sections at low inversion rates (as expected in cw lasers) are similar for the two polarizations and it is difficult to say from Fig. 6 which of them will dominate.

TABLE III. S_4 crystal field parameters, in cm^{-1}, for Tm^{3+} in NaLuW. The values in parentheses refer to estimated standard deviations of the indicated parameter. $\sigma=[\Sigma(\Delta_i)^2/(L-p)]^{1/2}$ with $\Delta_i=E_o-E_c$; L: number of levels; p: number of parameters included in the fit. Phenomenological free-ion parameters obtained in the S_4 fit for Tm^{3+} in $NaLu(WO_4)_2$, in cm^{-1}, $E^0=17610(1)$, $E^1=6731(3)$, $E^2=33.65(2)$, $E^3=669.8(2)$, $\alpha=14.080(6)$, $\beta=-645(7)$, $\gamma=[1800]$ taken as constant, $\zeta=2634.9(9)$, $M^0=3.85$, $M^2=0.56M^0$. $M^4=0.32M^0$, $P^2=700$, $P^4=0.75P^2$, $P^6=0.5P^2$.

	$NaLu(WO_4)_2$ (This work)	$CaWO_4$ (Ref. 16)	$LiTmF_4$ (Ref. 20)	$LiYF_4$ (Ref. 21)
B_0^2	312(12)	417.7	367	358.7
B_0^4	−675(25)	−687.7	−716	−607.8
B_4^4	±864(16)	753.6	918	844.2
B_0^6	−55(34)	17.1	−64	−173
B_4^6	±459(21)	504.3	615	629.2
S_4^6	±309(39)	359.2	118	0
σ	12.0	6.7	12	13.0

IV. LASER RESULTS

The initial cw laser experiments with Tm:NaLuW crystals were performed under Ti:sapphire laser (linewidth ~0.2 nm) pumping. The pump wavelength λ_{pump} was in all cases very close to the maximum absorption. Uncoated a-cut

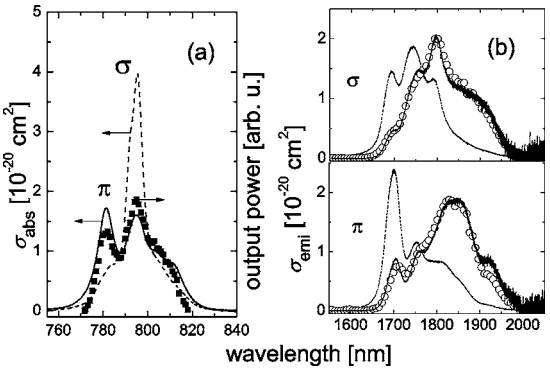

FIG. 5. Cross sections of Tm^{3+} in NaLuW. (a) Absorption cross sections of the $^3H_4$ multiplet for σ (dashed line) and π (solid line) polarizations. The excitation spectra recorded with the Tm:NaLuW laser (see next section) emitting at 1943 nm in π polarization (points) is included in arbitrary units for comparison. (b) Absorption (dashed line) and emission (solid line) cross sections of the $^3F_4$ multiplet. The $^3F_4$ photoluminescence (circles) is included for comparison.

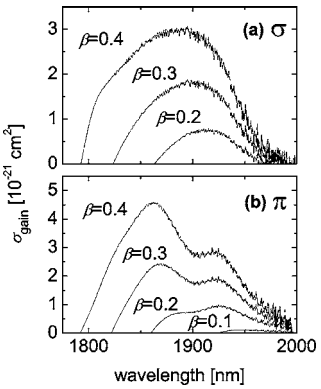

FIG. 6. Gain cross sections of Tm^{3+} in NaLuW for different inversion ratios, β. (a) σ polarization and (b) π polarization.

crystal plates were positioned at the Brewster angle, between the two focusing mirrors of the astigmatically compensated *X*-type cavity (total length of ~90 cm), shown in Fig. 7. Depending on the orientation of the crystal *c* axis, both σ and π polarizations were studied. The pump polarization was always in the same plane. M1, M2, and M3 mirrors were highly reflecting (>99.9%) from 1800 to 2075 nm and antireflection (AR) coated on the rear side for high transmission from 780 to 1020 nm. Output couplers (M4 in Fig. 7) with transmissions T_{OC}=1.5%, 3%, 5%, and 10%, were used. A single-plate intracavity Lyot filter (3 mm thick quartz plate with the optical axis at 60° to the surface) was employed for tuning. In the position of the Tm-doped crystal, the pump spot had a Gaussian waist of 37 μm.

Initially, the uncoated samples were simply fixed with one of their edges glued to a copper block without any special cooling.

When oriented for the σ polarization and higher pump absorption, the 0.94 mm thick, 11.72 mol % Tm-doped crystal studied first was prone to irreversible damage for incident pump powers of the order of 1 W. Therefore, the two polarizations were compared for this sample modulating the pump beam with a chopper (25% duty cycle). The slope efficiencies versus absorbed power were almost independent of the polarization (e.g., $\eta \approx 45\%$ with T_{OC}=5%). True cw operation was obtained with this sample only for π polarization: The maximum output power was ≈210 mW at a laser wavelength of λ_L=1961 nm for an absorbed power of ≈640 mW by using T_{OC}=1.5%, with a threshold of 123 mW, while the

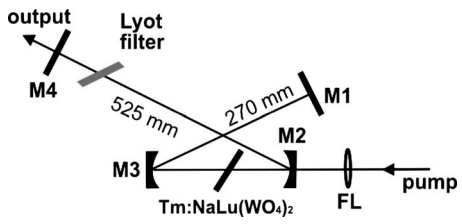

FIG. 7. Cavity setup of the Tm:NaLuW laser with Ti:sapphire laser pumping. FL: AR-coated focusing lens with *f*=70 mm; M1: plane total reflector; M2–M3: RC=−100 mm mirrors; M4: plane output coupler. For tuning experiments, a single-plate birefringent filter (Lyot filter) was introduced into the cavity under Brewster angle.

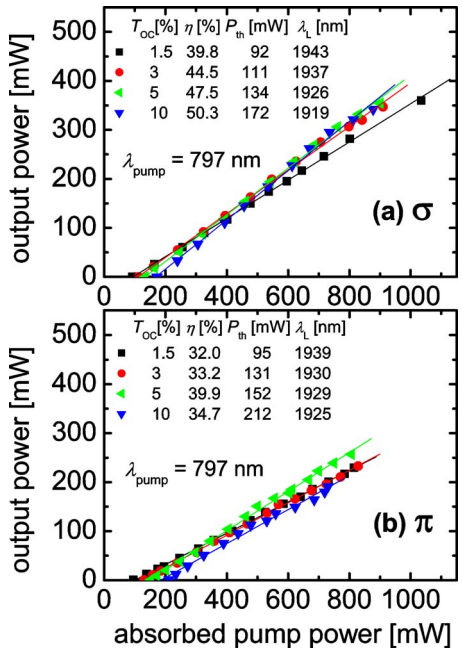

FIG. 8. (Color online) Input-output characteristics of the cw Tm:NaLuW laser without cooling using a 5.86 mol % doped sample with a thickness of 1.29 mm: (a) σ polarization and (b) π polarization. The symbols show the experimental points and the straight lines are fits for calculation of the slope efficiency η.

slope efficiency remained unchanged (e.g., $\eta \approx 45\%$ with T_{OC}=5%). The cw laser was tunable from 1824 to 1999 nm with T_{OC}=3%.

A 5.86 mol % Tm-doped sample with a thickness of 1.29 mm operated under true cw conditions for both polarizations. The results are summarized in Fig. 8 versus absorbed pump power. This sample had lower absorption and the results for σ polarization were somewhat better even if calculated against the absorbed pump power. The maximum slope efficiency for this polarization exceeded 50% with T_{OC}=10% [Fig. 8(a)]. The maximum output power reached 360 mW at 1943 nm by using T_{OC}=1.5%, while the threshold for this output coupler was only P_{th}=92 mW. The actual crystal absorption only slightly depended on the output coupling but it was different from the case without lasing due to the dependence of the pump saturation intensity on the intracavity laser intensity for the Tm^{3+} three-level system. Without lasing, the absorption was substantially lower than the low signal values: it roughly dropped from 85% to 65% for the σ polarization and from 65% to 55% for the π polarization, when the incident pump power reached 1.4 W.

By keeping the doping level unchanged (5.86 mol %) but using a sample with increased thickness (2.14 mm), we obtained yet higher output powers and slope efficiencies (Fig. 9). In this case, the absorption was also bleached at higher pump levels but this effect was almost totally suppressed in the presence of lasing. The results in Fig. 9 are thus presented against the actual absorbed power, exactly as in Fig. 8. The maximum output power reached 435 mW (T_{OC}=3%) at λ_L=1924 nm for π polarization, for which the pump absorption was also higher. In the σ polarization, the slope efficiency η exceeded 58% for T_{OC}=10% at a wavelength as short as 1922 nm (π polarization). Comparing with

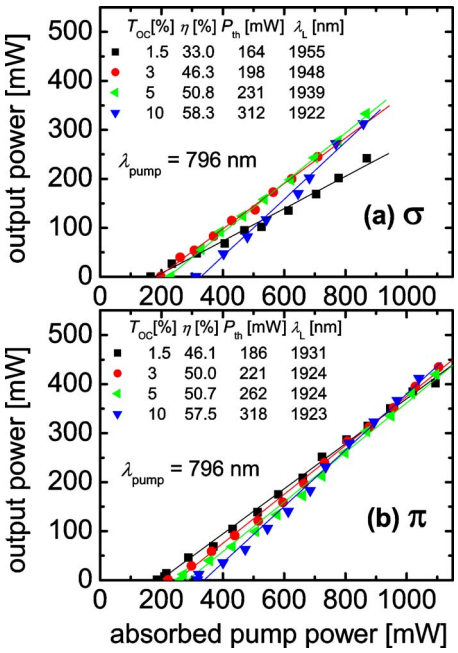

FIG. 9. (Color online) Input-output characteristics of the cw Tm:NaLuW laser without cooling using a 5.86 mol % doped sample with a thickness of 2.14 mm: (a) σ polarization and (b) π polarization. The symbols show the experimental points and the straight lines are fits for calculation of the slope efficiency η.

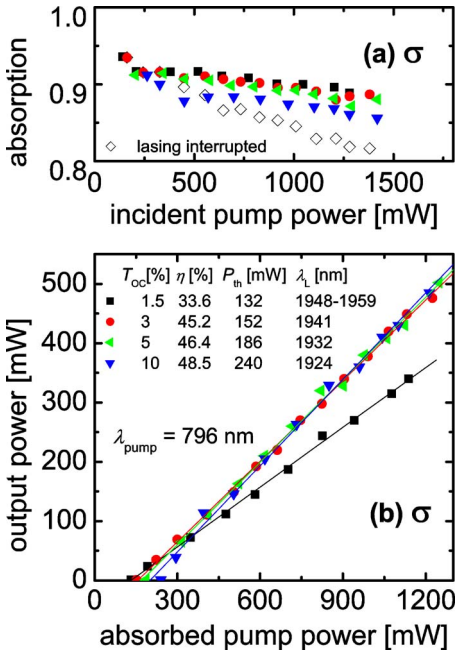

FIG. 10. (Color online) (a) Crystal absorption vs incident pump power and (b) input-output characteristics of the cw Tm:NaLuW laser for σ polarization using a 5.86 mol % doped sample with a thickness of 1.72 mm and water cooling.

Fig. 8, one can see that the performance of the π polarization has considerably improved. However, from the comparison of the two polarizations in Fig. 9, whose performance obviously depends on the doping level, sample thickness, and saturation effects, it is impossible to conclude which of them exhibits higher gain at equal pump conditions and compare to the computed gain curves in Fig. 6.

In an attempt to see the effect of reducing the thermal load to the crystal by heat removal, we prepared additional a-cut samples with an aperture of 4×3 mm^2 that were fixed in a water cooled copper holder in lateral contact. The concentration was the same, 5.86 mol %, and the thickness was 1.72 mm. The results for the σ polarization, together with the measured dependence of the crystal absorption, are shown in Fig. 10. The maximum output power obtained with this sample increased to 502 mW with the 5% output coupler. This corresponds to an optical-to-optical efficiency of 40.2% with respect to the absorbed pump power. The performance with the three output couplers with T_{OC}=3%, 5%, and 10% was very similar in terms of slope efficiency above the threshold and without any sign of rollover with increasing pump power. The slope efficiencies and the performance, in general, were similar to those depicted in Fig. 8(a) for the 1.29 mm thick sample. Although similar improvement of the results was achieved also for π polarization, in this case, as with the 1.29 mm thick sample, the performance of the σ polarization was better. Note that this was not the case with the thickest sample of 2.14 mm (Fig. 9).

A characteristic of the Tm:NaLuW laser is the wide spectral range of excitation wavelengths. Figure 5(a) shows the π-polarized laser output power of the 1.29 mm sample of 5.86 mol % Tm-doped NaLuW for an incident power of 975 mW and T_{OC}=1.5%. The laser excitation spectrum closely matches the corresponding absorption.

The tuning results obtained with the different samples using the intracavity Lyot filter are summarized in Fig. 11. The overall tunability achieved (from 1799 to 2026 nm at the zero level) and the broadest full width at half maximum (FWHM) (125 nm) are comparable to the results obtained with Tm:NaGdW.[5] The 125 nm bandwidth would support sub-50-fs near 1950 nm in the mode-locked regime. The trends that can be seen from Fig. 11 are that the tuning range shifts to longer wavelengths with increased optical density of the sample and that the σ polarization provides, in general, broader tunability. The effect of changing the output coupler transmission is clear from the results presented in Figs. 8–10. Higher losses require higher inversion rates, which, in the three-level Tm^{3+} laser system, means shifting to shorter oscillation wavelengths, which is in accordance with the calculated gain cross sections in Fig. 6.

By comparing the results achieved in the present work with Ti:sapphire laser pumping of Tm:NaLuW with the performance of the Tm:NaGdW laser[5] (note that the Tm:NaLaW laser had inferior performance[9]) it is clear that, at comparable thresholds, much higher slope efficiencies were achieved with Tm:NaLuW, leading to significant increase of the output power. Also, no rollover could be seen in the power dependence for Tm:NaLuW; in contrast, this effect was always present in the Tm:NaGdW laser.[5] When compared to the performance of the ordered monoclinic Tm:KLuW using the same setup, it should be outlined that the maximum slope efficiency and corresponding threshold (60.1% and 125 mW for T_{OC}=5% $E\|N_m$ in a 3.7 at. % Tm:KLuW) are only slightly better than those presently reported and that the tuning range was narrower

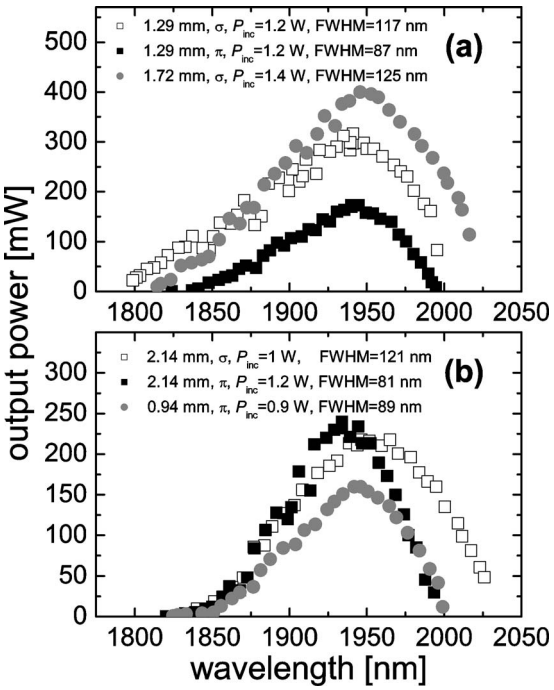

FIG. 11. Tunability of the cw Tm:NaLuW laser with the T_{OC}=3% output coupler. (a) σ and π polarizations for a 1.29 mm thick sample and σ polarization for a 1.72 mm thick and cooled sample of Tm:NaLuW, (b) σ and π polarizations for a 2.14 mm thick sample and π polarization for a 0.94 mm thick Tm:NaLuW sample. The 1.29, 1.72, and 2.14 mm thick samples are with 5.86 mol % Tm doping while the 0.94 mm thick sample is with 11.72 mol % doping. The sample thickness, pump and laser polarizations, incident pump power P_{inc}, and FWHM of the tuning curves are indicated in the figures.

(1800–1987 nm) despite that the ordered crystal could be pumped at higher levels (2.4 W of absorbed power) and the maximum output level when tuning was above 1 W.[24] This shows the improvement in laser tuning induced by the local disorder in NaLuW crystal. The comparison with other Tm-doped laser hosts is less significant because of the differences in experimental setup; nevertheless, the maximum efficiency achieved under Ti:sapphire laser pump in Tm-doped yttrium aluminum garnet (YAG) (59% and 390 mW for T_{OC}=5% in a 12 at. % Tm:YAG) (Ref. 25) was similar to that presently reported for Tm:NaLuW, while those obtained under diode pumping usually show lower slope efficiency and higher laser threshold although the final laser output is higher due to the larger available power in the diode laser source, see, for instance, the case of $LnVO_4$ (Ln=Y, Gd, and Lu).[26]

Comparing samples with different optical densities with the setup from Fig. 7, it was not possible to conclude which polarization exhibits higher gain under the same pumping conditions. For this purpose, we tested the three samples (the 1.29, 1.72, and 2.14 mm thick crystals) under normal incidence in a simple two-mirror hemispherical cavity. The output coupler with 3% transmission had a radius of curvature RC=−5 cm, and the samples were positioned close to the plane mirror. The same pump source was used (tuned to 796 nm), which was focused through the plane in-coupling mirror. With all three samples, the naturally selected polarization was parallel to the *c* axis (π), but the contrast was not perfect (roughly 5:1). This is contrary to the situation with Tm:NaGdW, where the polarization in the absence of selective elements was σ.[5] However, the imperfect polarization aspect means that under different conditions (crystal and pump parameters), one cannot rule out the possibility that competition of the two polarizations takes place for *a*-cut samples. The spectroscopic properties and the gain cross sections, in particular, are similar for the different hosts of that type, and it can be expected that such competition of the polarizations may be a general property. This means that high power schemes which are pumped by diode lasers would require, independent of the crystal cut of the active element, a polarizing component or surface for a defined polarization state. On the other hand, the close gain cross sections for the two polarizations means that the crystal cut could be selected on the basis of other arguments such as the thermal conductivity which is at present unknown for the NaLuW host.

V. CONCLUSION

Based on low temperature spectroscopic studies supported by a crystal field energy level fit procedure, we determined the Γ_2 IR for the ground $^3H_6(0)$ level of Tm^{3+} in NaLuW and the IRs of other excited Stark levels. This permitted to assign, in the S_4 site symmetry, the observed bands to specific electric dipole electronic transition, with the exception of the $^3H_6 \rightarrow {}^3H_5$ transitions which show polarization rules indicative of a non-negligible magnetic dipole contribution. A large number of bands experimentally observed at 5 K correspond to transitions from the first $^3H_6(1)$, $\Gamma_{3,4}$ excited level. The reliable determination of the $^3H_6$ and $^3F_4$ Stark levels allowed us to calculate the corresponding partition functions, which are necessary for the evaluation of the emission and gain cross sections for the Tm^{3+} transition responsible of laser action around 1.95 μm.

This first laser study of Tm-doped NaLuW, using a Ti:sapphire laser as a pump source, showed efficient performance at room temperature. The slope efficiencies achieved are one of the highest for Tm lasers and ≈500 mW of output power was obtained at modest pump levels (<1.5 W incident power). The tunability achieved (227 nm at zero level) is very promising for various applications requiring tunable laser radiation near 1.95 μm as well as for future mode-locking experiments. The laser experiments revealed that, for the present operating conditions, the polarization which dominates in the absence of selective elements is the one parallel to the optic axis. The laser was not very sensitive to the pump wavelength which could be varied by a few nanometers due to the broad absorption feature of Tm:NaLuW.

This work was supported by Project No. MAT2005-6354-C03-01 (Spain). J. M. Cano-Torres, X. Han, and M. Rico were supported by the Spanish Science and Education Ministry through I3P-BPD2005, Juan de la Cierva, and Ramón y Cajal grants, respectively. X. Mateos was supported by the Access to Research Infrastructures activity in the Sixth Framework Programme of the EU (Contract No. RII3-CT-2003-506350, Laserlab Europe). The experimental contributions of C. Kränkel and K. Petermann (Hamburg

University) in lifetime measurements and those of F. J. Valle (CSIC) in the measurement of the Tm concentration are also acknowledged.

[1]A. A. Kaminskii, Laser Photonics Rev. **1**, 93 (2007).
[2]C. Cascales, M. D. Serrano, F. Esteban-Betegón, C. Zaldo, R. Peters, K. Petermann, G. Huber, L. Ackermann, D. Rytz, C. Dupré, M. Rico, J. Liu, U. Griebner, and V. Petrov, Phys. Rev. B **74**, 174114 (2006).
[3]A. García-Cortés, J. M. Cano-Torres, X. Han, C. Cascales, C. Zaldo, X. Mateos, S. Rivier, U. Griebner, V. Petrov, and F. J. Valle, J. Appl. Phys. **101**, 063110 (2007).
[4]A. García-Cortés, J. M. Cano-Torres, M. D. Serrano, C. Cascales, C. Zaldo, S. Rivier, X. Mateos, U. Griebner, and V. Petrov, IEEE J. Quantum Electron. **43**, 758 (2007).
[5]J. M. Cano-Torres, M. D. Serrano, C. Zaldo, M. Rico, X. Mateos, J. Liu, U. Griebner, V. Petrov, F. J. Valle, M. Galán, and G. Viera, J. Opt. Soc. Am. B **23**, 2494 (2006).
[6]Yu. K. Voron'ko, K. A. Subbotin, D. A. Lis, A. V. Popov, A. A. Sobol, S. N. Ushakov, and E. V. Zharikov, Opt. Spectra **100**, 602 (2006); [Opt. Spektrosk. **100**, 656 (2006)].
[7]E. V. Zharikov, D. A. Lis, A. V. Popov, K. A. Subbotin, S. N. Ushakov, A. V. Shestakov, and I. Razdobreev, Quantum Electron. **36**, 515 (2006).
[8]H. Wang, G. Jia, F. Yang, Y. Wei, Z. Lou, Y. Wang, J. Li, Z. Zhu, X. Lu, and C. Tu, Appl. Phys. B: Lasers Opt. **83**, 579 (2006).
[9]J. M. Cano-Torres, X. Han, A. García-Cortés, M. D. Serrano, C. Zaldo, F. J. Valle, X. Mateos, S. Rivier, U. Griebner, and V. Petrov, Mater. Sci. Eng., B **146**, 22 (2008).
[10]Y. Wei, C. Tu, H. Wang, F. Yang, G. Jia, Z. You, J. Li, Z. Zhu, and Y. Wang, Appl. Phys. B: Lasers Opt. **86**, 529 (2007).
[11]X. Lu, Z. You, J. Li, Z. Zhu, G. Jia, B. Wu, and C. Tu, Opt. Mater. (Amsterdam, Neth.) **29**, 849 (2007).
[12]L. D. Merkle, J. B. Gruber, M. D. Seltzer, S. B. Stevens, and T. H. Allik, J. Appl. Phys. **72**, 4269 (1992).
[13]E. Cavalli, C. Meschini, A. Toncelli, M. Tonelli, and M. Bettinelli, J. Phys. Chem. Solids **58**, 587 (1997).
[14]X. Han, A. García-Cortés, M. D. Serrano, C. Zaldo, and C. Cascales, Chem. Mater. **19**, 3002 (2007).
[15]C. Cascales, A. Méndez-Blas, M. Rico, V. Volkov, and C. Zaldo, Opt. Mater. (Amsterdam, Neth.) **27**, 1672 (2005).
[16]D. E. Wortman, C. A. Morrison, and R. P. Leavitt, Phys. Rev. B **12**, 4780 (1975).
[17]M. Rico, V. Volkov, C. Cascales, and C. Zaldo, Chem. Phys. **279**, 73 (2002).
[18]A. Méndez-Blas, M. Rico, V. Volkov, C. Zaldo, and C. Cascales, Phys. Rev. B **75**, 174208 (2007).
[19]C. Cascales and C. Zaldo, Chem. Mater. **18**, 3742 (2006).
[20]H. P. Christensen, Phys. Rev. B **19**, 6573 (1979).
[21]H. P. Jenssen, A. Linz, R. P. Leavitt, C. A. Morrison, and D. E. Wortman, Phys. Rev. B **11**, 92 (1975).
[22]B. F. Aull and H. P. Jenssen, IEEE J. Quantum Electron. **18**, 925 (1982).
[23]K. Petermann, D. Fagundes-Peters, J. Johannsen, M. Mond, V. Peters, J. J. Romero, S. Kutovoi, J. Speiser, and A. Giesen, J. Cryst. Growth **275**, 135 (2005).
[24]X. Mateos, V. Petrov, J. Liu, M. C. Pujol, U. Griebner, M. Aguiló, F. Díaz, M. Galán, and G. Viera, IEEE J. Quantum Electron. **42**, 1008 (2006).
[25]R. C. Stoneman and L. Esterowitz, Opt. Lett. **15**, 486 (1990).
[26]R. Lisiecki, P. Solarz, G. Dominiak-Dzik, W. Ryba-Romanowski, M. Sobczyk, P. Černý, J. Šulc, H. Jelínková, Y. Urata, and M. Higuchi, Phys. Rev. B **74**, 035103 (2006).